PHYSICAL REVIEW A **92**, 031401(R) (2015)

Attosecond time-resolved streaked photoemission from Mg-covered W(110) surfaces

Qing Liao and Uwe Thumm
Department of Physics, Kansas State University, Manhattan, Kansas 66506, USA
(Received 16 December 2014; published 8 September 2015)

We formulate a quantum-mechanical model for infrared-streaked photoelectron (PE) emission by ultrashort extreme ultraviolet (XUV) pulses from an adsorbate-covered metal surface, exposing the influence of microscopic PE dispersion in substrate and adsorbate on the interpretation of streaked photoemission spectra and photoemission time delays. We validate this numerical model first by reproducing measured relative photoemission delays (a) between valence-band and $2p$-core-level (CL) PEs emitted from clean Mg(0001) surfaces and (b) between conduction-band (CB) and $4f$-CL PEs from clean W(110) surfaces at two XUV-pulse central photon energies. Next, applying this model to ultrathin Mg adsorbate layers on W(110) substrates, we reproduce (i) the measured nonmonotonic dependence of relative photoemission delays between CB and Mg($2p$) PEs and (ii) the monotonic dependence of relative delays between W($4f$) and Mg($2p$) PEs in a recent experiment [S. Neppl *et al.*, Nature (London) **517**, 342 (2015)].

DOI: 10.1103/PhysRevA.92.031401 PACS number(s): 32.80.Fb, 42.50.Hz, 42.65.Re, 79.60.−i

I. INTRODUCTION

The first proof-of-principle attosecond streaking experiment with a solid target [1] has opened the door to the time-resolved observation of electron transport in and near solids. In this experiment, a relative streaking time delay $\Delta\tau_{4f-\mathrm{CB}} = \Delta\tau_{4f} - \Delta\tau_{\mathrm{CB}} = 110 \pm 70$ as was measured for photoemission from localized W($4f$) core levels (CLs) and delocalized conduction-band (CB) levels of a W(110) surface [2]. The photoemission processes were induced by attosecond extreme ultraviolet (XUV) pulses with a central photon energy of 91 eV and streaked by a few-cycle infrared (IR) laser pulse. The large relative streaking delay was interpreted as being due to different transport properties of XUV-released photoelectrons (PEs) inside the solid within different classical [1,3] and quantum-mechanical numerical [4,5] models. More recently, smaller relative delays $\Delta\tau_{4f\text{-CB}} = 55 \pm 10$ and 28 ± 14 as were deduced for atomically flat W(110) surfaces at XUV central energies of 94 and 118 eV, respectively [6]. In addition, a much smaller delay of $\Delta\tau_{2p\text{-VB}} = 5 \pm 20$ as was measured [7] between the photoemission from valence-band (VB) levels and $2p$ CLs of a Mg(0001) surface.

Metals differ with regard to their electron mean-free path (MFP), group velocity, localization character of initial-state wave functions, and screening of an external IR streaking field. With regard to the contrast in wave-function localization of Mg($2p$) CL and Mg VB states, compared with the smaller contrast of W($4f$) CL and W(CB) states, one might expect $\Delta\tau_{2p\text{-VB}}$ to exceed $\Delta\tau_{4f\text{-CB}}$ [8]. However, the opposite behavior found both experimentally [1,7] and theoretically [9,10], $\Delta\tau_{2p\text{-VB}} < \Delta\tau_{4f\text{-CB}}$, indicates that energy-dependent MFPs and the screening of the IR streaking field at the surface overcompensate the effect of the wave-function-localization contrast on relative photoemission time delays. In addition, while Mg can be modeled as a free-electron metal [7,11], the representation of the PE dispersion in W is less obvious. Previous studies of the influence of energy dispersion on the photoemission time delay focused on the group velocity [1,3,12]. Since the final PE states are coherent superpositions of PE wave packets released from different layers, streaked PE spectra and photoemission delays depend on the relative phases between the superimposed PE wave packets, i.e., on momenta and dispersion of PEs *inside* the solid. Besides the photoemission time delay, the spectrograms contain information about the spectral bandwidth and chirp of the exciting attosecond XUV pulse [9,10]. Thus, a quantum-mechanical model that can not only incorporate all of the above contributions to the photoemission time delay, but also reproduce the characteristics of the streaking spectrograms, is undoubtedly needed for a comprehensive understanding of laser-assisted single-XUV-photon photoemission processes from solids.

A recent prototypical experiment with ultrathin Mg films grown on a W(110) substrate [11] demonstrated the dependence of streaked PE spectra and relative photoemission delays on PE-transport effects in the adsorbate and across the adsorbate-substrate interface. This experiment revealed a monotonic increase with the adsorbate-film thickness of the relative photoemission delay $\Delta\tau_{4f\text{-}2p}$ between electrons emitted from the substrate-$4f$ and adsorbate-$2p$ levels, while the relative time delay $\Delta\tau_{\text{CB-}2p}$ between electrons emitted from the CB of the Mg/W(110) system and adsorbate-$2p$ electrons was observed to depend in a nonmonotonic way on the Mg-film thickness. Since Mg($2p$) and W($4f$) CL electrons are localized at atomic cores, W($4f$) PEs have to traverse the Mg film. Therefore a significant part of the accumulated delay $\Delta\tau_{4f\text{-}2p}$ can be estimated classically, based on energy conservation and the film thickness d. Photoemission from the $2p$ level of a 1 ML Mg adsorbate thus provides an excellent reference for photoemission time delays from substrate levels with regard to addressing substrate-adsorbate-interface and electron-propagation effects in streaked photoemission spectra.

The observed initial-state and adsorbate-thickness dependence of streaked photoemission from Mg-covered W(110) substrates motivated the composition and scrutiny of the general quantum-mechanical model discussed in this Rapid Communication, which is organized as follows. We describe our theoretical model in Sec. II, present and discuss numerical results for Mg(0001), W(110), and Mg-covered W(110) surfaces in Sec. III, and add our conclusions in Sec. IV. Unless stated otherwise, we use atomic units throughout this Rapid Communication.

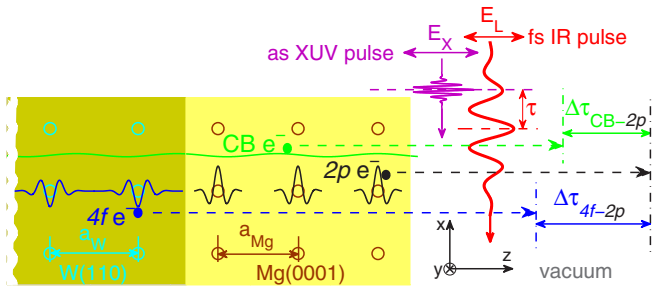

FIG. 1. (Color online) Schematic of attosecond streaking spectroscopy from the Mg/W(110) adsorbate-substrate system.

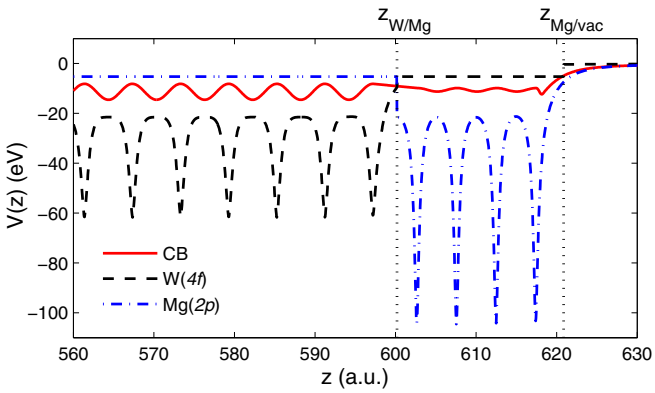

FIG. 2. (Color online) Effective potentials for conduction-band and W($4f$) and Mg($2p$) core-level electrons for a 4 ML Mg/W(110) adsorbate-substrate system.

II. THEORETICAL MODEL

IR-laser-streaked PE emission by attosecond XUV pulses from metal-adsorbate systems is shown schematically in Fig. 1. The grazingly incident XUV and IR pulses are linearly polarized in the plane of incidence (x-z plane). The XUV electric field can be assumed to have an infinite skin depth since the photocurrent is limited by a comparatively short PE MFP [5]. The IR electric field is screened at the metal surface with a very small skin depth comparable to the lattice spacing [7,11]. CL and CB electrons are released by adsorbing one XUV photon. During their propagation along the surface-normal direction (z axis) towards the metal-vacuum interface, the amplitudes of released PE wave packets decrease due to elastic and inelastic scattering with other electrons and atomic cores. After laser-free propagation inside the solid, PE wave packets are streaked by the IR pulse close to the metal-vacuum interface. Variation of the delay τ between the XUV and IR pulses thus encodes the photoemission time in streaked PE spectrograms in terms of observable periodic PE energy shifts [1,2,5]. PEs emitted from different locations arrive at different times at the interface and thus acquire different energy shifts in the IR streaking field. This leads to a broadening of the PE energy distribution at any given delay between the XUV and IR pulses.

For photoemission along the surface normal direction, the interaction between the active electron and the XUV electric field $E_X(t)$ can be described in first-order perturbation theory in the dipole-length gauge [10]. The photoemission transition amplitude is then given by [5]

$$T_{\mathbf{k}_f,\mathbf{k}_i}(\tau) \propto \int dt \int dz\, \psi_f(z,t)^* E_X(t) z \psi_i(z,t), \qquad (1)$$

where $\psi_i(z,t) = \psi_i(z)e^{-i\varepsilon_i t}$ is an occupied initial state with binding energy ε_i. From the observable photoemission probability, $P(E_f,\tau) = \sum_i |T_{\mathbf{k}_f,\mathbf{k}_i}(\tau)|^2$ for final kinetic energies $E_f = k_f^2/2$, we compute the centers of energy of the streaking traces from W($4f$), Mg($2p$), and occupied CB states, respectively. Taking the phase of the IR vector potential $A_L(t)$ as a reference, this allows us to extract "*absolute*" streaking time delays, $\Delta\tau_{4f}$, $\Delta\tau_{2p}$, and $\Delta\tau_{\mathrm{CB}}$, for W($4f$), Mg($2p$), and CB emission, respectively [9].

A. Generalized Volkov states

The IR electric field is modeled to be screened with skin depth $\delta_L = 2$ Å [4,9,11] measured from the metal-vacuum interface position $z_{\mathrm{Mg/vac}}$ (Fig. 2) or $z_{\mathrm{W/vac}}$ (for adsorbate-free W surfaces). For such a small skin depth, we approximate the IR intensity to be constant for $z > z_{\mathrm{Mg/vac}} - \delta_L$ and to vanish for $z < z_{\mathrm{Mg/vac}} - \delta_L$. We approximate the final PE state as the generalized Volkov wave function

$$\psi_f(z,t) = f(\lambda_{\mathrm{W}},\lambda_{\mathrm{Mg}};z)\, e^{i\int_\infty^z dz' p(z')} \times e^{i[\omega_X(t)+\varepsilon_i][t_1(z)-t]} e^{i\phi_v(t_1(z),k_f)}, \qquad (2)$$

which takes the screening of the external IR streaking field inside solids into account. With the factor

$$f(\lambda_{\mathrm{W}},\lambda_{\mathrm{Mg}};z) = \begin{cases} e^{-(z_{\mathrm{W/Mg}}-z)/(2\lambda_{\mathrm{W}})-d/(2\lambda_{\mathrm{Mg}})}, & z < z_{\mathrm{W/Mg}} \\ e^{-(z_{\mathrm{Mg/vac}}-z)/(2\lambda_{\mathrm{Mg}})}, & z_{\mathrm{W/Mg}} \leqslant z < z_{\mathrm{Mg/vac}} \\ 1, \quad z \geqslant z_{\mathrm{Mg/vac}}, \end{cases} \qquad (3)$$

we model the damping of the PE wave function inside the adsorbate-substrate system, with reference to the W-Mg interface position $z_{\mathrm{W/Mg}}$ and metal-vacuum interface position $z_{\mathrm{Mg/vac}}$ (Fig. 2). The energy-dependent MFP values for W and Mg, λ_{W} and λ_{Mg}, respectively, are taken from experiments [6,7] or calculations [13] (Table I). For all numerical applications in this work, the film thickness $d = z_{\mathrm{Mg/vac}} - z_{\mathrm{W/Mg}}$ exceeds the IR skin depth δ_L.

The phase accumulation for different release locations is described by the factor $e^{i\int_\infty^z dz' p(z')}$ in Eq. (2). This expression generalizes the exponential $e^{i[k_f+A_L(t'-\tau)]z}$ in ordinary Volkov wave functions [5], taking the presence of the adsorbate-covered surface into account. Since $k_f \gg A_L$, we can approximate $p(z') = k_f$ for $z' \geqslant z_{\mathrm{Mg/vac}}$. $p(z')$ is determined by the

TABLE I. Electron mean-free paths, λ_{Mg} and λ_{W}, in Mg and W metals, respectively. λ_{W} at ~60 eV is calculated [13]. All other mean-free-path values are determined experimentally [6,7]. m_e^* is the effective electron mass in W used in this work.

Energy (eV)	~60	~68	~87	~115
λ_{Mg} (Å)		3.7	4.2	4.9
λ_{W} (Å)	5.0		3.9	3.6
m_e^* (a.u.)	1		1	0.86

respective PE dispersion relations inside the substrate (for $z' < z_{\mathrm{W/Mg}}$) and inside the adsorbate (for $z_{\mathrm{W/Mg}} \leqslant z' < z_{\mathrm{Mg/vac}}$). The factor $e^{i[\omega_X(t)+\varepsilon_i][t_1(z)-t]}$ in Eq. (2) describes the phase accumulated without the IR laser field after one-XUV-photon ionization at time t to the onset of streaking at time $t_1(z)$. The XUV frequency $\omega_X(t)$ is time dependent due to the chirp of the attosecond pulse. $\phi_v(t_1(z),k_f) = \frac{1}{2}\int_{t_1(z)}^{\infty} dt'[k_f + A_L(t'-\tau)]^2$ is the *delayed* Volkov phase. In contrast to the ordinary Volkov phase [5] it depends on the coordinate z due to the screening of the IR field inside the solid. Based on the group velocities $v_g = dE_f(p)/dp$ in different regions, we classically calculate the time in the phase of the Volkov wave function,

$$t_1(z) = \begin{cases} t + \frac{z_{\mathrm{W/Mg}}-z}{v_g(\mathrm{W})} + \frac{d-\delta_L}{v_g(\mathrm{Mg})}, & z < z_{\mathrm{W/Mg}} \\ t + \frac{z_{\mathrm{Mg/vac}}-\delta_L-z}{v_g(\mathrm{Mg})}, & z_{\mathrm{W/Mg}} \leqslant z < z_{\mathrm{Mg/vac}} - \delta_L \\ t, & z \geqslant z_{\mathrm{Mg/vac}} - \delta_L, \end{cases} \quad (4)$$

when a PE released at position z at time t arrives at the position $z_{\mathrm{Mg/vac}} - \delta_L$ of the onset of streaking.

We use the experimental laser- and XUV-pulse parameters [11], assuming XUV electric-field pulses $E_X(t) \propto e^{-2\ln 2(t/\tau_X)^2} e^{-i\omega_X(t)t}$ of length $\tau_X = 435$ as, $\omega_X(t) = \omega_{Xc} + \beta_X t$, central photon energy $\hbar\omega_{Xc} = 118$ eV, and chirp parameter $\beta_X = -2$ fs^{-2}. The IR pulse with a peak intensity of 10^{11} W/cm^2 is given by the vector potential $A_L(t) = A_0 e^{-2\ln 2(t/\tau_L)^2}\cos(\omega_L t)$ with length $\tau_L = 5$ fs and photon energy $\hbar\omega_L = 1.5$ eV.

B. Effective valence- and conduction-band potentials

1. No adsorbate

We first construct an effective potential for W(110) CB electrons based on a slab with 200 W atoms by adjusting the lattice spacing $a_{\mathrm{W}} = 3.16$ Å [14] and the four independent parameters $A_{10}(\mathrm{W})$, $A_1(\mathrm{W})$, $A_2(\mathrm{W})$, and $\beta(\mathrm{W})$ in the Chulkov single-active-electron potential [15]. $A_{10}(\mathrm{W})$ determines the position of the energy gap in the valence electronic spectrum of W(110), $A_1(\mathrm{W})$ the width of the energy gap, and $A_2(\mathrm{W})$ and $\beta(\mathrm{W})$ the energies of the surface and first image states. We adjust $A_{10}(\mathrm{W}) = -11.35$ eV and $A_1(\mathrm{W}) = 3.2$ eV, in order to reproduce the measured energy-gap position and width (between -0.8 and -4 eV relative to the Fermi level [6,16,17]). To reproduce the measured surface-state energy at -1.3 eV [16,18] relative to the Fermi level and the first image-state energy [19], and to define the image-plane position $z_{\mathrm{im}}(\mathrm{W})$ at 4.14 ($> a_{\mathrm{W}}/2$) above the topmost W nucleus, we employ the values $A_2(\mathrm{W}) = 1.4$ eV and $\beta(\mathrm{W}) = 3.3$.

2. One to four adsorbate monolayers

Ultrathin Mg(0001) adsorbate films grown on a W(110) surface have been studied extensively in photoemission experiments [17,20–23] and phase-accumulation models [17,20]. They support discrete quantum-well states [24], suggesting highly reflective W-Mg and Mg-vacuum interfaces.

We model the joint CB potential of the Mg/W(110) system as a combination of the above Chulkov parametrization for the adsorbate-free W(110) CB potential and a quantum-well potential for the Mg film, based on the following assumptions: (i) For Mg-adsorbate thicknesses between one and four monolayers (MLs), the work function of Mg/W(110) is equal to the work function $W_F(\mathrm{W}) = 5.25$ eV of W(110) [25]. (ii) The spacing $a_{\mathrm{Mg}} = 2.61$ Å between two adjacent Mg atoms is the same as in bulk Mg crystals. (iii) The spacing between two adjacent W and Mg atoms at the interface is $a_{\mathrm{W}}/2 + a_{\mathrm{Mg}}/2$, and $z_{\mathrm{W/Mg}}$ is defined at $a_{\mathrm{W}}/2$ above the topmost W nucleus.

3. One adsorbate monolayer

The valence potential for a 1 ML Mg film is modeled by the soft-core Coulomb potential $U_{\mathrm{SC}} = -1/\sqrt{z^2+7.5}$, which reproduces the ionization energy (7.65 eV) of isolated Mg atoms [26]. We represent the effective potential of the joint CB for 1 ML Mg/W(110) within the Chulkov model for W(110) inside the substrate ($z < z_{\mathrm{W/Mg}}$) and by U_{SC} inside the adsorbate, including a reflective drop in potential energy of 1.4 eV at the substrate-adsorbate interface $z_{\mathrm{W/Mg}}$.

4. Two to four adsorbate monolayers

For 2–4 ML coverage, we model the valence potentials by a Chulkov potential with a modified potential-depth parameter $A_{10}(\mathrm{Mg})$ [27]. Since streaked photoemission experiments [11] revealed characteristic Mg plasmon-loss peaks in the CB spectrum for $\geqslant 4$ MLs of Mg on W(110), we approximate the potential depth of 4 ML Mg films by the bulk potential-depth parameter $A_{10}(\mathrm{Mg}) = -10.55$ eV in the Mg(0001) Chulkov potential [15]. Based on the workfunction $W_F(\mathrm{Mg}) = 3.66$ eV of bulk Mg(0001) [27], we assume a linear increase of the potential depth by $W_F(\mathrm{Mg})/3$ per ML, resulting in $A_{10}(\mathrm{Mg}) = -9.33$ eV and $A_{10}(\mathrm{Mg}) = -8.11$ eV for 3 and 2 ML Mg coverage, respectively. We parametrize the joint CB effective potentials for 2–4 ML Mg/W(110) systems by the W(110) Chulkov potential inside the substrate and by the Mg(0001) Chulkov potential inside the adsorbate. Across the W-Mg interface interval, $[z_{\mathrm{W/Mg}} - a_{\mathrm{W}}/2, z_{\mathrm{W/Mg}} + a_{\mathrm{Mg}}/2]$, the two Chulkov potentials are connected linearly as shown by the red solid line in Fig. 2 for 4 ML Mg/W(110). The resulting adsorbate quantum wells support discrete states in the z direction for 1–4 ML Mg coverage. We define $z_{\mathrm{Mg/vac}} = z_{\mathrm{im}}(\mathrm{Mg})$ 1.83 Å above the topmost Mg nucleus [15].

5. 30 adsorbate monolayers (bulk limit)

For 30 ML Mg coverage on W(110), the joint CB photoemission is dominated by emission from the Mg(0001) VB. It was shown experimentally that the electronic properties of the VB of a 30 ML Mg adsorbate are indistinguishable from single-crystalline Mg(0001) [28]. We therefore use a freestanding slab of 30 Mg atoms to model the 30 ML Mg adsorbate, based on the Mg(0001) Chulkov potential [15], which reproduces the measured VB electronic properties [9].

C. Effective core-level potentials

Since W(4f) and Mg(2p) CL electrons are confined in deep potential wells with binding energies of 31.3 and 49.6 eV relative to the respective Fermi levels, we model the CL potentials for W(4f) and Mg(2p) electrons independently, by adding the Yukawa potential $U_Y(z) = \sum_j -e^{-|z-z_j|/\xi}/\sqrt{(z-z_j)^2 + a_0^2}$ to the W(110) CB and Mg(0001) VB potentials, respectively [4,9] (Fig. 2). z_j denotes lattice points. ξ and

TABLE II. Streaked photoemission time delays for conduction-band and W($4f$) and Mg($2p$) core-level photoelectrons, relative to the phase of the streaking-field vector potential, as functions of the Mg coverage on a W(110) substrate.

Delay(as) \ Cov.(ML)	0	1	2	3	4
$\Delta\tau_{CB}$	24	19	51	88	81
$\Delta\tau_{4f}$	52	96	146	191	240
$\Delta\tau_{2p}$		2	19	31	40

a_0 are adjusted to 3 and 0.294 for Mg($2p$) and to 3 and 0.52 for W($4f$), respectively. With these values we reproduce the measured central binding energies and narrow bandwidths of 0.9 and 0.7 eV, close to the measured values of ∼0.6 [7] and ∼0.6 eV [6], respectively.

III. NUMERICAL RESULTS AND DISCUSSION

A. Mg(0001) surfaces

We first apply our numerical model to a freestanding slab of 30 Mg atoms. Assuming free-electron dispersion [$E_f(p) = p^2/2$] with $v_g \simeq p = k_{fz}$, 118 eV XUV central energy, and measured MFPs of 4.9 and 3.7 Å for VB and $2p$ CL PEs, respectively [7] (see Table I), we obtain $\Delta\tau_{2p\text{-VB}} = -11$ as (Table II). This relative streaking delay overlaps the measured delay range of 5 ± 20 as [7] (Fig. 4). Changing the CB-MFP values by ±1Å does not noticeably change the absolute CB-photoemission delay, while shifts of about 3 as per 0.1 Å MFP change occur for CL emission [9,10].

B. W(110) surfaces

Next, we apply our numerical model to W(110) surfaces at different XUV central energies. In tungsten, the energy dispersion is less obvious than in the more free-electron-like magnesium. Angle-resolved photoemission spectroscopy cannot measure energy dispersion along the normal direction [29] and *ab initio* band-structure calculations [1,12] disagree at the PE energies relevant for this work. Lacking reliable *ab initio* band-structure calculations, we access the microscopic effect of energy dispersion by employing an effective-mass (m_e^*) approximation, $E_f(p) = p^2/(2m_e^*)$ [30]. Nevertheless, assuming free-electron dispersion ($m_e^* = 1$) for both W($4f$) and W(CB) PEs near 60 and 87 eV, respectively, corresponding to $\hbar\omega_{Xc} = 94$ eV, our model yields a relative photoemission delay of $\Delta\tau_{4f\text{-CB}} = 66$ as for a MFP of released CB electrons of 5 Å [13] and a MFP of released W($4f$) electrons of 3.9 Å [6], respectively, in good agreement with the measured delay of 55 ± 10 as [6].

The 118 eV XUV pulse releases ∼87 eV W($4f$) and ∼115 eV W(CB) PEs. The corresponding measured W($4f$) and CB PE MFPs are 3.9 and 3.6 Å [6], respectively. If we use free-electron dispersion ($m_e^* = 1$) for W($4f$) PEs, our model predicts an *absolute* streaking time delay of $\Delta\tau_{4f} = 52$ as. For ∼115 eV W(CB) PEs, free-electron dispersion yields $\Delta\tau_{CB} = 68$ as, failing to reproduce the measured *relative* delay $\Delta\tau_{4f\text{-CB}} = 28 \pm 14$ as [6]. Adjusting $m_e^* = 0.86$ (increasing the PE group velocity v_g by 8% and PE momenta by 7%, compared to free electrons at equal energy) reduces $\Delta\tau_{CB}$ to 24 as and yields the measured relative delay $\Delta\tau_{4f\text{-CB}} = 28$ as. This reduction is mainly due to the change of PE momenta inside W; increasing v_g by 8% reduces $\Delta\tau_{CB}$ by only 5 as.

C. Adsorbate-covered Mg(0001)/W(110) surfaces

Figures 3(c) and 3(d) show our calculated streaked PE spectra for 1 and 4 ML Mg coverage on W(110) by 118 eV XUV pulses. The MFP of W($4f$) PEs, with energies of ∼87 eV when entering the Mg film, is inferred to be $\lambda_{Mg} = 4.2$ Å from the approximately linear relation between MFP and electron kinetic energy for 40–200 eV PEs [7]. Our calculated streaked spectra agree well with the experimental data [Figs. 3(a) and 3(b)] [11] with regard to (i) the energetic position, width, and oscillation amplitude of the streaking trace; (ii) conspicuous τ-dependent changes in the streaking trace (i.e., of the PE temporal and spectral shape) due to the negative chirp of the XUV pulse [7,9]; and (iii) qualitatively, the relative change in PE yield with d.

Our calculated *absolute* streaking time delays for CB, W($4f$), and Mg($2p$) PEs are shown in Table II. Compared to the clean W(110) surface, adsorption of one atomic Mg layer almost does not change $\Delta\tau_{CB}$. This is consistent with measured synchrotron photoemission spectra showing almost no effect on CB photoemission due to the addition of 1 ML Mg on a W substrate [6,17]. The increase of $\Delta\tau_{CB}$ with the adsorbate thickness d can be attributed to (i) more PEs being emitted from the free-electron Mg adsorbate and (ii) PEs released within the substrate needing increasingly more travel time. As discussed above, free-electron dispersion results in a larger streaking delay than using $m_e^* = 0.86$. This trend reverses for >3 MLs, since fewer PEs released within the substrate can

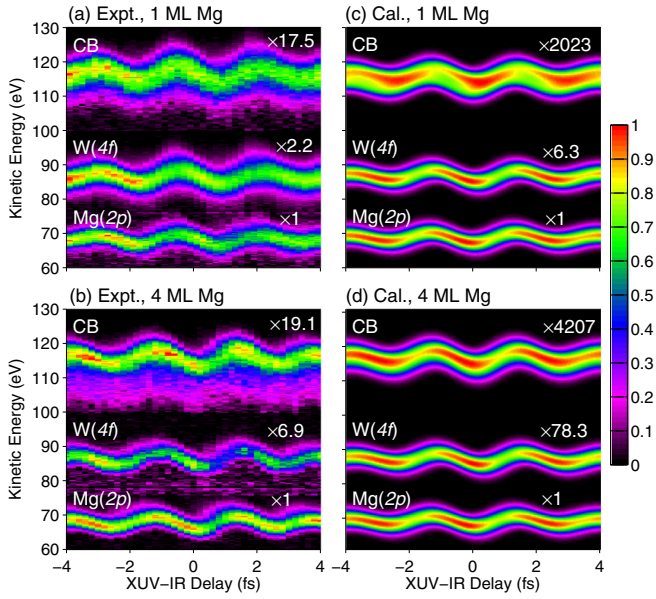

FIG. 3. (Color online) (a), (b) Measured [11] and (c), (d) calculated attosecond streaking spectrograms for photoemission from conduction-band and W($4f$) and Mg($2p$) core levels of Mg/W(110). (a), (c) 1 ML and (b), (d) 4 ML Mg coverage.

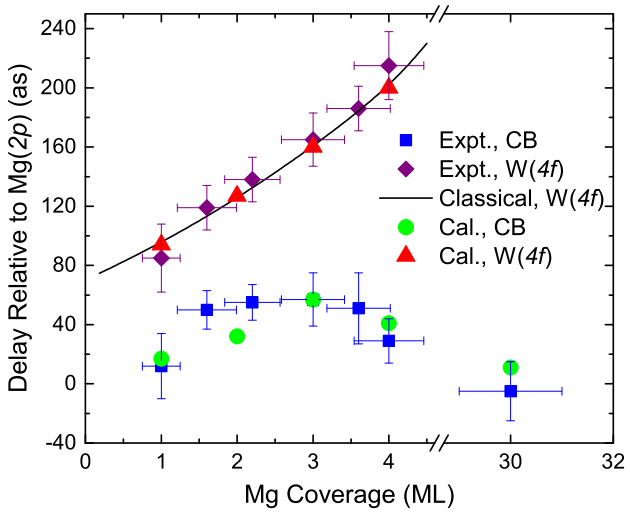

FIG. 4. (Color online) Streaking time delays relative to Mg($2p$) emission for conduction-band and W($4f$) photoelectrons, $\Delta\tau_{\text{CB-}2p}$ and $\Delta\tau_{4f\text{-}2p}$, respectively, as a function of the Mg coverage. Blue squares and purple diamonds: measured values [7,11]. Green circles and red triangles: present quantum-mechanical calculations. Solid line: classical free-electron calculations [11].

escape into vacuum. $\Delta\tau_{\text{CB}}$ now decreases towards the delay $\Delta\tau_{\text{VB}}$ from bulk Mg(0001), consistent with the measured [11] CB streaking trace beginning to exhibit characteristic bulk Mg(0001) plasmon loss [7] for 4 ML Mg adsorbate thickness. Our results in Fig. 4 show the same overall trend in the dependence of the *relative* delay $\Delta\tau_{\text{CB-}2p}$ on the adsorbate thickness as the measurements [11].

In contrast to CB PEs, W($4f$) electrons localized inside the substrate must travel an additional distance d. For 87 eV W($4f$) PEs this geometrical estimate yields an added travel time of 47 as per ML Mg coverage, matching the average absolute streaking delay per ML in our quantum-mechanical calculation (Table II). Our calculated thickness-dependent relative photoemission time delays $\Delta\tau_{4f\text{-}2p}$ in Fig. 4 agree with recent experimental data [11] and a classical free-electron model [11]. This classical model assumes $\delta_L = 0$ at the adsorbate-vacuum-interface position $z_{\text{Mg/vac}}$, located at a distance $a_{\text{Mg}}/2$ above the topmost Mg atom, and uniform electron density inside the solids.

The differences in $\Delta\tau_{4f\text{-}2p}$ between the nominal measured values [11] (disregarding error bars on the purple diamonds in Fig. 4) and our calculations are -9, 5, 5, and 15 as for 1–4 ML Mg/W(110), respectively. Adjusting a_{Mg} to the measured relative streaking delays induces changes of -0.50, 0.14, 0.09, and 0.31 Å (or -19, 5, 3.5, and 7.9%) in the assumed monolayer thickness of 1–4 ML thick adsorbate films (the negative value means reduced thickness). This can be interpreted as an expression of competing attractive forces exerted on Mg atoms by Mg and W atoms [22]: by adding Mg monolayers, the Mg-Mg attraction better competes with the Mg-W attraction, stretching the Mg-W interfacial width.

IV. CONCLUSIONS

We have validated a general quantum-mechanical model for attosecond streaking spectroscopy of heterogeneous condensed matter systems. Our modeling of PE dispersion in W in free-electron approximation ($E = p^2/2$) at kinetic energies near 87 eV and in effective-mass approximation ($E = p^2/2m_e^*$, $m_e^* = 0{,}86$) near 115 eV, reproduces the measured monotonic increase of $\Delta\tau_{4f\text{-}2p}$ and non-monotonic behavior of $\Delta\tau_{\text{CB-}2p}$ with adsorbate thickness. This, in turn, supports our dispersion modeling and emphasizes the importance of PE-energy-dependent electron-propagation effects. Our results indicate that attosecond streaking spectroscopy can serve as a powerful tool not only to time resolve electronic dynamics in condensed matter systems, but also to explore on an atomic length scale the electronic and morphological properties of thin films and solid-solid interfaces, pointing to the use of streaked electron spectroscopy as a diagnostic instrument for heterogeneous semiconductor structures.

ACKNOWLEDGMENTS

We thank S. Neppl for providing the experimental data. This work was supported in part by NSF Grant PHY 1068752, the Chemical Sciences, Geosciences, and Biosciences Division, Office of Basic Energy Sciences, Office of Science, US DOE, and the Alexander von Humboldt Foundation.

[1] A. L. Cavalieri, N. Müller, Th. Uphues, V. S. Yakovlev, A. Baltuška, B. Horvath, B. Schmidt, L. Blümel, R. Holzwarth, S. Hendel, M. Drescher, U. Kleineberg, P. M. Echenique, R. Kienberger, F. Krausz, and U. Heinzmann, Nature (London) **449**, 1029 (2007).

[2] U. Thumm, Q. Liao, E. M. Bothschafter, F. Süßmann, M. F. Kling, and R. Kienberger, in *Handbook of Photonics Vol. 1: Attosecond physics*, edited by D. L. Andrew (Wiley, New York, 2015).

[3] C. Lemell, B. Solleder, K. Tőkési, and J. Burgdörfer, Phys. Rev. A **79**, 062901 (2009).

[4] A. K. Kazansky and P. M. Echenique, Phys. Rev. Lett. **102**, 177401 (2009).

[5] C.-H. Zhang and U. Thumm, Phys. Rev. Lett. **102**, 123601 (2009); **103**, 239902(E) (2009).

[6] S. Neppl, Ph.D. thesis, Technische Universität München, 2012.

[7] S. Neppl, R. Ernstorfer, E. M. Bothschafter, A. L. Cavalieri, D. Menzel, J. V. Barth, F. Krausz, R. Kienberger, and P. Feulner, Phys. Rev. Lett. **109**, 087401 (2012).

[8] C.-H. Zhang and U. Thumm, Phys. Rev. A **84**, 065403 (2011).

[9] Q. Liao and U. Thumm, Phys. Rev. Lett. **112**, 023602 (2014).

[10] Q. Liao and U. Thumm, Phys. Rev. A **89**, 033849 (2014).

[11] S. Neppl, R. Ernstorfer, A. L. Cavalieri, C. Lemell, G. Wachter, E. Magerl, E. M. Bothschafter, M. Jobst, M. Hofstetter, U. Kleineberg, J. V. Barth, D. Menzel, J. Burgdörfer, P. Feulner, F. Krausz, and R. Kienberger, Nature (London) **517**, 342 (2015).

[12] E. E. Krasovskii, Phys. Rev. B **84**, 195106 (2011).
[13] S. Tanuma, C. J. Powell, and D. R. Penn, Surf. Interface Anal. **17**, 911 (1991).
[14] N. W. Ashcroft and N. D. Mermin, *Solid State Physics* (Cornell University, Ithaca, NY, 1976).
[15] E. V. Chulkov, V. M. Silkin, and P. M. Echenique, Surf. Sci. **437**, 330 (1999).
[16] A. M. Shikin, A. A. Rybkina, A. S. Korshunov, Yu. B. Kudasov, N. V. Frolova, A. G. Rybkin, D. Marchenko, J. Sánchez-Barriga, A. Varykhalov, and O. Rader, New J. Phys. **15**, 095005 (2013).
[17] N. A. Vinogradov, D. E. Marchenko, A. M. Shikin, V. K. Adamchuk, and O. Rader, Phys. Solid State **51**, 179 (2009).
[18] K. Miyamoto, A. Kimura, K. Kuroda, T. Okuda, K. Shimada, H. Namatame, M. Taniguchi, and M. Donath, Phys. Rev. Lett. **108**, 066808 (2012).
[19] U. Thomann, Ch. Reuß, Th. Fauster, F. Passek, and M. Donath, Phys. Rev. B **61**, 16163 (2000).
[20] C. Koitzsch, C. Battaglia, F. Clerc, L. Despont, M. G. Garnier, and P. Aebi, Phys. Rev. Lett. **95**, 126401 (2005).
[21] F. Schiller, R. Keyling, E. V. Chulkov, and J. E. Ortega, Phys. Rev. Lett. **95**, 126402 (2005).
[22] L. Aballe, A. Barinov, A. Locatelli, T. O. Mentes, and M. Kiskinova, Phys. Rev. B **75**, 115411 (2007).
[23] A. M. Shikin and O. Rader, Phys. Rev. B **76**, 073407 (2007).
[24] U. Thumm, P. Kürpick, and U. Wille, Phys. Rev. B **61**, 3067 (2000).
[25] R. W. Strayer, W. Mackle, and L. W. Swanson, Surf. Sci. **34**, 225 (1973).
[26] V. Kaufman and W. C. Martin, J. Phys. Chem. Ref. Data **20**, 83 (1991).
[27] H. B. Michaelson, J. Appl. Phys. **48**, 4729 (1977).
[28] F. Schiller, M. Heber, V. D. P. Servedio, and C. Laubschat, Phys. Rev. B **70**, 125106 (2004).
[29] S. Hüfner, *Photoelectron Spectroscopy: Principles and Applications*. 3rd ed. (Springer, Berlin, 2003).
[30] J. M. Luttinger and W. Kohn, Phys. Rev. **97**, 869 (1955).